Publ. Astron. Obs. Belgrade No. 107 (2025), 69 - 74 *Talk*
http://doi.org/10.69646/14sbac10p

COLUMN DENSITY DISTRIBUTIONS FROM DECOMPOSED MAPS OF STAR-FORMING REGIONS

L. MARINKOVA[1], T. V. VELTCHEV[2], S. DONKOV[3]

[1] *Department of Applied Physics, Faculty of Applied Mathematics, Technical University-Sofia, 8 Kliment Ohridski Blvd., Sofia 1000, Bulgaria*
E–mail: ln@phys.uni-sofia.bg

[2] *University of Sofia, Faculty of Physics, 5 James Bourchier Blvd., 1164 Sofia, Bulgaria*

[3] *Institute of Astronomy and NAO, Bulgarian Academy of Sciences, 72 Tsarigradsko Chausee Blvd., 1784 Sofia, Bulgaria*

Abstract. Probability distribution functions of mass- (ρ-PDF) and column density (N-PDF) in star-forming regions often display one or multiple power-law tails (PLT) in the high-density range. The correct PLT extraction is of key significance for understanding morphological and dynamical structure of star-forming regions since the PDF properties can be directly linked to the role of different factors in the star formation process: gravity, turbulence, magnetic fields, etc. Many observations indicate that the PLT regime in the N-PDF corresponds to highly fragmented, filamentary regions in a star-forming cloud - thus, it is interesting to compare N-PDFs of small-scale structures extracted in those areas with the N-PDF of the whole cloud. We present analyses of the N-PDFs in Galactic regions of various star-forming activity obtained from Herschel data, by use of a novel method (Li 2022) for decomposion of a map into multiple components containing structures of different sizes.

1. INTRODUCTION

Molecular clouds and/or their fragments associated with some star formation activity are usually labeled star-forming regions (SFRs). They exhibit highly complex structure: clumps of various density, hub-filament systems hosting pre-/protostellar cores (Kumar et al. 2020, Zhou et al. 2022), H II regions around newborn massive stars and dust lanes. Contraction and collapse in SFRs on multiple physical scales and take place in the context of interplay of gravity, turbulence and magnetic fields (Chevance et al. 2020) as gravity governs the formation and growth of dense gas structures.

An increasingly popular tool to assess the physical conditions and processes in SFRs is the analysis of the probability distribution functions of mass- (ρ-PDF) and column density (N-PDF). Isothermal, non-gravitating medium dominated by supersonic turbulence is characterized by a lognormal ρ-PDF (i.e. normal distribution of logdensity; e.g., Federrath, Klessen & Schmidt 2008) while the development of high-density power-law tail (PLT) of the distribution is typically due to the increasing role of self-gravity in contracting clouds (Kritsuk, Norman & Wagner 2011, Federrath & Klessen 2012, 2013). At later evolutionary times, at the stage of local collapses, the PLT slope becomes shallower and tends toward a constant value as substantiated theoretically (Girichidis et al. 2014) and confirmed by numerical simulations (e.g.,

Veltchev et al. 2019). N-PDFs obtained from high-resolution observations of SFRs display similar shapes like the ρ-PDFs. The main part is (quasi-)lognormal or a combination of two lognormals while a single (Kainulainen et al. 2009) or even double PLT (Schneider et al. 2015, 2022) appear at the high-density end.

In view of the multi-scale nature of the star-forming process and of the cloud evolution in general, it is critically important to quantify the contribution of different spatial scales to the PDF shape. In analytical or numerical analysis of the ρ-PDF, this can be done, for instance, attributing effective sizes by some density cutoff (see Donkov, Veltchev & Klessen 2012). However, the N-PDF of an observed SFRs is a result of various projection effects of complex structures and straightforward approaches are not applicable. A method to decompose N-PDFs to contributions of different abstract spatial scales in the cloud have been suggested by Stanchev et al. (2015); it starts by extracting the PLT and then fitting the main part of the distribution by combination of lognormals. Their approach is based on specific assumptions about cloud physics: the PLT range is attributed to gravoturbulent regime while the main PDF part is attributed to predominantly turbulent regime.

In this report we present some preliminary results from another, essentially different approach of decomposition of N-PDFs in several Galactic SFRs of various activity. It makes use of a method for multiscale decomposition of astronomical maps recently suggested by G.-X. Li (2022) which allows to dissentagle the physical scales accounting for the observed PLTs.

2. DECOMPOSITION OF MAPS AND N-PDFs

Typical maps of SFRs obtained from high-resolution observations reveal a bunch of structures with different characteristic sizes. Robust decomposition of such maps into components of multiple scales enables new approaches to data analysis – for example, study of the relative importance of filaments and cores.

The method of G.-X. Li (2022) produces a set of smoothed images $I_k(x, y)$ from an input map $I_0(x, y)$ through a modified version of wavelet transformation. (For more information, we refer the reader to the original paper and the references therein.) The wavelet kernel defines the spatial scale in pixels $l = 2^k$, where $k = 1, 2, ..., k_{\max}$ and $2^{k_{\max}}$ is the larger side of the input rectangular map. As the scale increases with k, the intensity $I_k(x, y)$ decreases monotonically with k. Now one can construct decomposed maps $C_k = I_{k-1} - I_k$ which contain structures with size between 2^{k-1} and 2^k pixels. Correspondingly, the input map can be recovered through summation over the decomposed ones:

$$I_0(x, y) = \sum_k C_k(x, y) + I_{k_{\max}}(x, y) \quad , \tag{1}$$

where the residual $I_{k_{\max}}(x, y)$ is significant only in regions of very low intensities (column densities).

This technique can be used to assess the contribution of structures with some typical size to a studied part of the N-PDF. Let us consider a pixel from the input map. Its column density is equal to the sum of column densities from the decomposed maps (eq. 1). The total number of all pixels from the input map $I_0(x, y)$ with column densities $\log N \leq \log N' < \log N + \Delta \log N$ yields the value of the N-PDF $P(\log N)$

in the considered bin. Accordingly, the relative contribution f_k of structures with sizes between 2^{k-1} and 2^k pixels to $P(\log N)$ is obtained through summation over all pixels from C_k corresponding to the pixels with $\log N'$ from $I_0(x, y)$:

$$f_k(\log N) = \frac{\sum\limits_{N' \in [\log\ N, \log\ N + \Delta\ \log\ N)} C_k(x, y)}{\sum\limits_{N' \in [\log\ N, \log\ N + \Delta\ \log\ N)} I_0(x, y)} \quad . \tag{2}$$

3. DATA USED

We extract and analyze high-density N-PDFs from *Herschel* maps constructed from convolved SPIRE maps (at 500, 350 and 250 μm) of 8 SFRs initially studied by Schneider et al. (2022). The high angular resolution ($18''$) allows for resolve the high-density part of the N-PDF which is accounted for mostly by clumps and cores on parsec and subparsec scales. The emission of the dust has been converted to A_V assuming a power-law for dust opacity in the far infrared and a gas-to-dust ratio of 100 (for details, see Veltchev et al. 2018, Sect. 2.2.) The PLTs are defined through:

$$P_{\rm PLT}(\log N) = C(N/N_0)^n \ , \tag{3}$$

where N_0 is some normalizing value (typically, the mean column density in the SFR) and C is a constant. The slopes $n < 0$ were extracted by the technique adapted BPLFIT (Veltchev et al. 2019, 2024) which provides the best fit of the presumed power-law part of the distribution without any presuppositions about its main part.

Table 1: Studied star-forming regions: some characteristics. Column 4 gives the lowest resolved scale (LRS)

SFR	**Distance** [kpc]	**Eff. size** ($A_V > 1$) [pc]	**LRS** [pc]	**PLT slopes** (from BPLFIT)
High-mass				
M 16	2.00	18.3	0.18	$n = -2.54$
M 17	2.20	28.1	0.18	$n_1 = -2.87$, $n_2 = -1.97$
Intermediate-mass				
Mon R2	0.86	5.1	0.10	$n_1 = -1.66$, $n_2 = -1.42$
Mon OB1	0.80	4.3	0.10	$n_1 = -1.89$, $n_2 = -3.62$
Low-mass				
Lupus III	0.16	1.3	0.02	$n = -2.21$
Lupus VI	0.20	1.5	0.02	$n_1 = -2.63$, $n_2 = -3.38$
Quiescent				
Musca	0.15	1.0	0.02	$n_1 = -2.17$, $n_2 = -5.75$
Polaris	0.49	1.9	0.06	$n = -4.32$

We studied SRFs with different activity and size (Table 1). The low-mass ones are clouds with masses $10^3 - 10^4\ M_\odot$ that typically give birth to low-mass stars while the high-mass regions are giant molecular clouds ($10^5 - 10^6\ M_\odot$) and observational signatures of high-mass star formation; they often contain gravitationally unstable

filamentary structures of high column density. In between these categories are SFRs with masses $10^4 - 10^5\ M_\odot$ where mainly low- and intermediate-mass stars emerge. Quiescent clouds are those with no or very little SF activity (up to a few protostars or prestellar cores) containing mostly atomic gas.

4. RESULTS

Figure 1 (top) dipslays the N-PDFs of the selected high- and intermediate-mass SFRs together with the column-density distributions from the decomposed maps C_k. The dynamic range of N (proportional to A_V) is large but the extracted PLTs correspond, in general, to $A_V \gtrsim 10$ (see the deviation points in dashed). Most of the N-PDFs from the decomposed maps have PLTs as well; typically of similar slope (plotted with solid black line). Comparison with the functions $f_k(A_V)$ reveals that a few dominating scales (DS) contribute to the PLT from the input map. This is evident in case of a single PLT (M 16) or for the *second* PLT when a double PLT is detected (M 17, Mon R2, Mon OB1). In the latter case, the first PLT is a result of various scales and probably cannot be associated with self-gravitating gas in dense compact clumps.

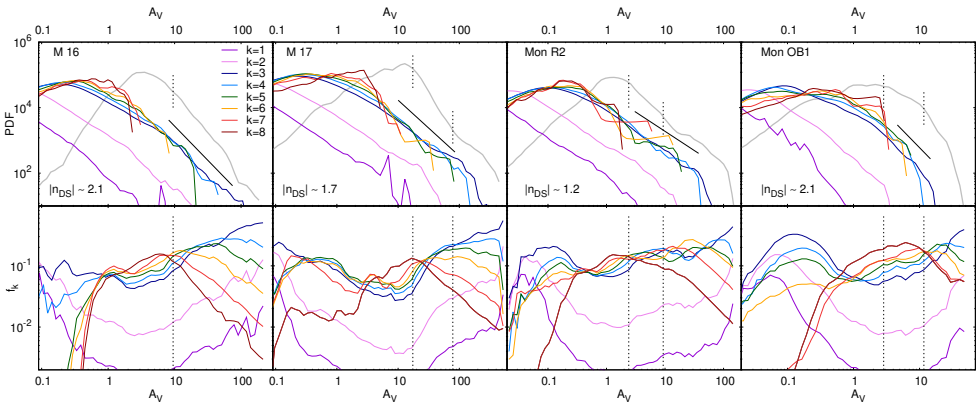

Figure 1: Decomposition of N-PDFs in the studied high- and intermediate-mass SFRs (See Table 1). The N-PDFs from the input map (thick grey line) and from C_k (color lines) are plotted in the top panel. The bottom panel dipslays the contributions f_k of structures with different size (eq. 2). The deviation points of the detected PLTs are shown (vertical dashed). The typical slope of the PLTs from the dominating scales ($n_{\rm DS}$) is given and drawn (black solid line in the top panels).

The picture in low-mass and quiescent SFRs seems to be more complicated (Fig. 2). N-PDFs from C_k do not have smooth PLTs. Various scales contribute to the single (Lupus III, Polaris) or the first PLT from the input map (Lupus VI, Musca). There are no clear dominating scales for the second PLT as well. In view of its high slope, one can argue that it is not real but can be rather interpreted as a resolution cutoff in zones of high extinction or other incompleteness effects.

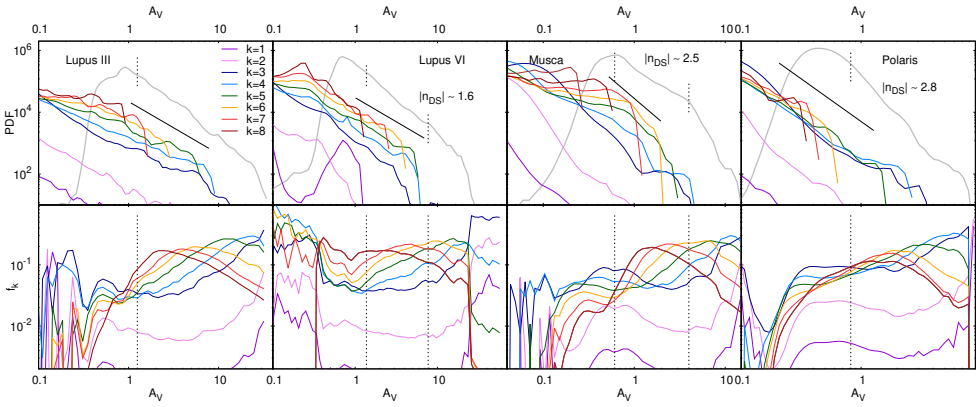

Figure 2: The same like Fig. 1 but for low-mass and quiescent SFRs.

5. SUMMARY

The novel method of map decomposition (G.-X. Li 2022) allows for distingushing the contribution of different spacial scales to the morphology of N-PDF in observed Galactic star-forming regions (SFRs). Preliminary analysis from a sample of *Herschel* maps of SFRs (Table 1) shows that:

- In high- and intermediate-mass SFRs the detected single PLTs result from contribution of a few dominating scales corresponding to structures with sizes $0.1 - 0.5$ pc. The same is true about the regime of a second detected PLT, while the first PLT results from contributions of wide range of scales and may be is not associated with self-gravitating structures.

- The typical slopes of PLTs $1.2 \leq |n| \leq 2.1$ from the maps C_k corresponding to the dominating scales ($k = 3 - 5$) are in general agreement with the theoretical expectations from density profiles of envelopes of collapsing protostellar cores (Larson 1969, Penston 1969, Donkov, Veltchev & Klessen 2017).

- Multiple scales of various size contribute to the detected PLTs in the studied low-mass and quiescent nearby SFRs. This hinders any clear physical interpretation.

Applying the method for map decomposition to G-Virial maps of SFRs by use of CO emission data (see the contribution of Mihaylov et al. in this volume) would allow to assess the gravitational boundedness of the structures at different scales and thus shed light at the physical picture behind the PLT phenomenon.

Acknowledgements

We acknowledge support by the Deutsche Forschungsgemeinschaft (DFG) under grant number KL 1358/20-3 and additional funding from the Ministry of Education and Science of the Republic of Bulgaria, National RI Roadmap Project DO1-326/4.12.2023.

References

Chevance, M., Kruijssen, J. M. D., Vazquez-Semadeni, E., Nakamura, F. et al. (2020). *Space Science Reviews*, **216**, Issue 4, article id. 50, doi: 10.1007/s11214-020-00674-x

Donkov, S., Veltchev, T. V., Klessen, R. S. (2017). *Monthly Notices of the Royal Astronomical Society*, **466**, 914., doi: 10.1093/mnras/stw3147

Federrath, C., Klessen, R. S. (2012). *Astrophysical Journal*, **761**, L156, doi: 10.1088/0004-637X/761/2/156

Federrath, C., Klessen, R. S. (2013). *Astrophysical Journal*, **763**, L51, doi: 10.1088/0004-637X/763/1/51

Federrath, C., Klessen, R. S., Schmidt, W. (2008). *Astrophysical Journal*, **688**, L79, doi: 10.1086/595280

Girichidis, P., Konstandin, L., Whitworth, A. P., Klessen, R. S. (2014). *Astrophysical Journal*, **781**, L91, doi: 10.1088/0004-637X/781/2/91

Kainulainen, J., Beuther, H., Henning, T., Plume, R. (2009). *Astronomy & Astrophysics*, **508**, 35, doi: 10.1051/0004-6361/200913605

Kritsuk, A., Norman, M., Wagner, R. (2011). *Astrophysical Journal*, **727**, L20, doi: 10.1088/2041-8205/727/1/L20

Kumar, M., Palmeirim, P., Arzoumanian, D., Inutsuka, S. I. (2020). *Astronomy & Astrophysics*, **642**, 87, doi: 10.1051/0004-6361/202038232

Larson, R. (1969). *Monthly Notices of the Royal Astronomical Society*, **145**, 271, doi: 10.1093/mnras/145.3.271

Li, G.-X., (2022). *Astrophysical Journal Supplement Series*, **259**, 59, doi: 10.3847/1538-4365/ac4bc4

Mihaylov, H., Stanchev, O., Veltchev, T. V. (2025). *Publ. Astron. Obs. Belgrade*, **107**, 75, doi: 10.69646/14sbac11p

Penston, M. V. (1969). *Monthly Notices of the Royal Astronomical Society*, **144**, 425., doi: 10.1093/mnras/144.4.425

Schneider, N., Bontemps, S., Girichidis, P., Rayner, T., Motte, F. et al. (2015). *Monthly Notices of the Royal Astronomical Society*, **453**, 41, doi: 10.1093/mnrasl/slv101

Schneider, N., Ossenkopf-Okada, V., Clarke, S., Klessen, R. S., Kabanovic, S., Veltchev, T. et al. (2022). *Astronomy & Astrophysics*, **666**, 165, doi: 10.1051/0004-6361/202039610

Stanchev, O., Veltchev, T. V., Kauffmann, J., Donkov, S., et al. (2015). *Monthly Notices of the Royal Astronomical Society*, **451**, 5575, doi: 10.1093/mnras/stv998

Veltchev, T., Girichidis, P., Donkov, S., Schneider, N. et al. (2019). *Monthly Notices of the Royal Astronomical Society*, **489**, 788, doi: 10.1093/mnras/stz2151

Veltchev, T., Girichidis, P., Marinkova, M., Donkov S. et al. (2024). *Monthly Notices of the Royal Astronomical Society*, **528**, 432., doi: 10.1093/mnras/stae031

Veltchev, T., Ossenkopf-Okada, V., Stanchev, O., Schneider, N., et al. (2018). *Monthly Notices of the Royal Astronomical Society*, **475**, 2215, doi: 10.1093/mnras/stx3267

Zhou, J.-W., Liu, T., Evans, N. J. et al. (2022). *Monthly Notices of the Royal Astronomical Society*, **514**, 603, doi: 10.1093/mnras/stac1735